JOURNAL OF AIRCRAFT
Vol. 42, No. 2, March–April 2005

Simulation of Helicopter Shipboard Launch and Recovery with Time-Accurate Airwakes

Dooyong Lee,* Nilay Sezer-Uzol,* Joseph F. Horn,† and Lyle N. Long‡
Pennsylvania State University, University Park, Pennsylvania 16802

A simulation of the helicopter/ship dynamic interface has been developed and applied to simulate a UH-60A operating from a landing helicopter assault (LHA) class ship. Steady and time-accurate inviscid computational-fluid-dynamics (CFD) simulations are performed over a full-scale LHA class ship using the parallel flow solver PUMA2 to predict the unsteady vortical ship airwake. Time-accurate CFD solutions of the LHA airwake are interfaced with a flight dynamics simulation based on the GENHEL model. The flight dynamics model was updated to include improved inflow modeling and gust penetration effects of the ship airwake. An optimal control model of a human pilot was used to simulate pilot control activity for a specified approach and departure trajectory. The pilot model was designed so that the tracking performance could be tuned based on a desired crossover frequency in each control axis. Results show that the unsteadiness of the ship airwake has significant impact on pilot workload when the helicopter is operating near the deck and superstructure of the ship.

Introduction

HELICOPTER shipboard launch and recovery operations continue to be a topic of interest for both civil and military operators. Ship-based helicopters regularly operate off rolling and pitching decks, in adverse weather conditions, and often within close proximity to the superstructure of the ship. Highly turbulent airwakes from the ship's superstructure, low visibility, and moving flight decks make helicopter shipboard operations one of the most challenging, training intensive, and dangerous of all helicopter flight operations.

To ensure the compatibility of a particular rotorcraft and ship under various operating conditions, extensive dynamic interface flight testing must be performed. This approach is limited by the availability of fleet assets and weather conditions. For example, the wind-over-deck (WOD) envelope defines the allowable wind conditions in terms of speed and azimuth for a given helicopter ship combination. The envelope is established by performing a series of flight tests for all possible combinations of wind speed and azimuth (typically in 5-kn, 15-deg increments) and taking subjective pilot ratings. The WOD envelopes are often overly restrictive because certain wind conditions never present themselves during tests.

Better simulation tools for analyzing shipboard operations might be used for a variety of purposes. Simulation testing can be used for pilot training and to reduce flight-test time and cost for establishing safe WOD envelopes. Ultimately pilot simulation testing might be used in acceptance testing of future rotorcraft and future ships.[1] In addition to the piloted simulation applications, the development of a non-real-time simulation tool for use in engineering and design would also be valuable. Such a simulation tool could be used to find optimal approach paths for safe landings, to design and test new flight control systems, and to identify possible trouble spots for future ship and helicopter combinations early in the design phase. Three key elements of this simulation tool include: computational-fluid-dynamics (CFD) representations of the time-varying ship airwake, a high-fidelity flight dynamics model of the helicopter, and a feedback control model of the human pilot.

Received 30 November 2003; revision received 24 June 2004; accepted for publication 2 July 2004.

*Graduate Research Assistant, Department of Aerospace Engineering.
†Assistant Professor, Department of Aerospace Engineering.
‡Professor, Department of Aerospace Engineering.

Understanding and modeling the ship airwake presents a number of technical challenges. Complex ship geometries (with superstructures and sharp edges), atmospheric boundary layers, atmospheric turbulence, and helicopter/ship airwake interactions all add to the complexity of the flowfield. Some of the key flow features of the airwake are unsteadiness, large regions of separated flow, vorticity, and low Mach number. Previous researchers have performed numerous experimental and computational studies of airwakes for different classes of ships. There have been some experimental investigations using both full-scale tests (which are costly and time consuming)[2] and scale-model tests in wind tunnels.[3–8] Computational simulations of ship airwakes have been performed using different numerical approaches by Tai,[9] Tattersall et al.,[10] Liu and Long,[11] Guillot and Walker,[12] and Reddy et al.[13] Recently, Sharma and Long[14] have simulated inviscid, steady and time-accurate flow over an LPD-17 ship using a modified parallel flow solver PUMA. They found good agreement between the steady-state solution and frequency spectrum of the wind-tunnel experiments. Polsky[2] and Polsky and Bruner[2,15] have investigated LHA class ship airwakes using the parallel unstructured flow solver COBALT with different numerical methods such as laminar Navier–Stokes and monotone integrated large-eddy simulation (MILES) approach as well as k–ω and shear-stress-transport (SST) turbulence modeling. It was shown that steady-state CFD calculations were unable to predict the time average of the turbulent flowfield, and it was observed that turbulence modeling added too much dissipation to the calculation because the flux-splitting numerical schemes are very dissipative. Bogstad et al.[16] have solved for inviscid flow around six different ships of the Royal Navy to obtain an airwake database for a helicopter flight simulator (Merlin). They incorporated the CFD-generated time-averaged airwake into the flight simulator. On the other hand, Zan[17] stated that the incorporation of the time-accurate airwake is important for a high-fidelity flight simulation. He also stated that for a reasonable validation of CFD the changes in the wind direction need to be considered. Camelli et al.[18] have performed an large-eddy simulation (LES) of airwake and stack gas temperature field around the landing platform dock (LPD)-17 class ship using a Smagorinsky turbulence model.

A number of recent research programs have also focused on the simulation of helicopter flight dynamics during shipboard operations, with the goal of assessing handling qualities and pilot workload. The Joint Shipboard Helicopter Integration Process (JSHIP) has been applied to increase the interoperability of joint shipboard helicopter operations for helicopters that are not specifically designed to go aboard Navy ships.[19–21] JSHIP was used to evaluate the compatibility, procedures, and training issues associated with integrating Army and Air Force helicopters with Navy ships. As

a part of JSHIP, the Dynamic Interface Modeling and Simulation System (DIMSS) was established to define and evaluate a process for developing WOD flight envelops. Using DIMSS, the fidelity standards for the shipboard launch and recovery task have been discussed for the combination of an LHA class ship and a UH-60 (Ref. 20) The helicopter shipboard operational limit prediction tool with coupled helicopter/ship aerodynamic interaction and integrated flight envelope analysis have been studied by He et al.[22] Inverse simulation techniques have also been applied to determine the pilot control input for shipboard launch and recovery operations.[23]

Over the last several decades, the extensive effort in developing feedback control theory has also proven to be quite useful in quantifying control-related human behavior.[24–26] The so-called crossover model employs classical control methods to model human feedback control of single-input/single-output (SISO) systems. The method is based on the expected crossover frequency of the open-loop transfer function of the human and controlled process. In fact, Bradley and Turner[25] applied the crossover model, coupled with inversion control methods, specifically to model pilot workload for helicopter shipboard operations. The main drawback of the crossover model is that the helicopter piloting task is inherently multi-input/multi-output (MIMO) system. Although extensions of the classical crossover model can be applied to MIMO systems, the use of modern MIMO control theory can be more convenient, particularly because the design algorithms are readily automated using modern software such as MATLAB®. The optimal control model (OCM) of the human pilot is applied for control of MIMO systems by solving the linear-quadratic-Gaussian problem. It has been shown that this approach had direct correlations with the classical crossover model, but is more readily applied to MIMO systems, and that the weighting coefficients can be derived based on desired crossover frequency.[26]

In this study, a dynamic-interface (DI) simulation of the UH-60A helicopter operating off an LHA ship is developed. This represents the same aircraft/ship combination used in the JSHIP program. The objective of this study is to understand the impact of a time-varying ship airwake on the pilot control activity for approach and departure operations. The model builds upon a previous analysis of the UH-60 operating near a generic frigate.[27] In that study, steady-state CFD solutions of the frigate airwake were coupled with an experimentally derived stochastic representation of the time-varying airwake.[28] The time-varying component of the airwake was assumed to be uniform over the entire body of the aircraft. In this study, the model of the helicopter/ship dynamic interface is modified to include time-accurate solutions of the ship airwake. The parallel unstructured maritime aerodynamics CFD solver (PUMA2) is used to calculate the flow over the LHA. Both the temporal and spatial variation of the unsteady wake are accounted for in the flight dynamics simulation. An optimal control model of a human pilot is used to simulate the pilot control inputs required to perform approach and departure operations, and the qualitative effects of time-varying ship airwake on pilot control activity are explored. The results show that the unsteadiness of the ship airwake has significant impact on pilot workload when the helicopter is operating near the deck and superstructure of the ship.

Helicopter/Ship Dynamic Interface Simulation Model

To simulate the helicopter/ship dynamic interface, it is necessary to model the kinematics, dynamics, and aerodynamics of the helicopter, the flight control system, the ship motion, and the airwake of the ship. The flight dynamics model is based on the GENHEL model of the UH-60A (Ref. 29). To facilitate model improvements and control law development, a MATLAB/SIMULINK-based version is developed. The code has been updated to include a high-order Peters-He inflow model,[30,31] and a special gust penetration model is developed to include the effects of ship airwake. CFD solutions can be used to provide steady-state or time-varying airwake velocities that result in local gust disturbances at various locations on the helicopter. It is also possible to use a combination of steady-state CFD solutions and a stochastic representation of the time-varying component of velocity. The gust penetration model extends previous research on ship airwake and atmospheric turbulence disturbances on helicopters.[27,32,33] To simulate approach and departure trajectories, an optimal control model of a human pilot has been developed. This controller acts as an outer-loop controller to simulate pilot inputs for a specified trajectory.

Ship Airwake Model—CFD Flow Solver

The helicopter simulation is integrated with time-accurate CFD solutions of the airwake of an LHA class ship. The PUMA2 is used to calculate the flow. It uses a finite volume formulation of the Euler/Navier–Stokes equations for three-dimensional, internal and external, nonreacting, compressible, steady/unsteady solutions for complex geometries. PUMA2 can be run so as to preserve time accuracy or as a pseudounsteady formulation to enhance convergence to steady state. It is written in ANSI C using the message-passing-interface library for message passing so that it can be run on parallel computers and clusters. It is also compatible with C++ compilers and coupled with the computational steering system POSSE.[34,35] It uses dynamic memory allocation; thus, the problem size is limited only by the amount of memory available on the machine. Large-eddy simulations can also be performed with PUMA2 (Refs. 34, 36, and 37).

Helicopter Flight Dynamic Model

The simulation model is divided into submodules that represent the aerodynamics and dynamics of the main rotor, fuselage, empennage, and tail rotor. Each of these components comprises points that are located at some distance relative to the center of gravity of the helicopter. The total forces and moments are calculated from a sum of the aerodynamic, mass, and inertia forces acting on each component. The simulation uses a total force, large-angle representation of the six rigid-body degrees of freedom (DOF) of the fuselage. The main rotor module includes rigid rotor-blade flapping, lagging, and rotational degrees of freedom as well as an air mass degree of freedom. In this study, the model was updated to include a high-order Peters-He inflow model.

This Peters-He inflow model is based on an acceleration potential with a skewed cylindrical wake. The flowfield and the rotor lift are expanded in terms of appropriate inflow modes. The induced flow is expressed azimuthally by a Fourier series and radially by Legendre functions. The magnitude of each term is determined from first-order ordinary differential equations in either the time or frequency domain, with blade lift as the forcing function.[30] In this paper, a 15-state inflow model is used.

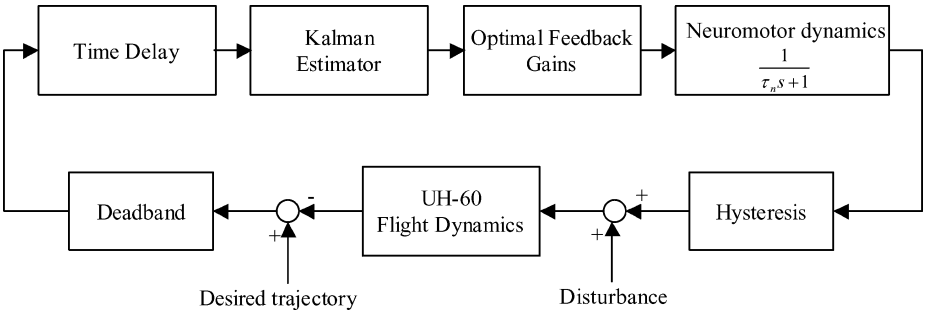

Fig. 1 Optimal control model of a human pilot.

The flight control system consists of the primary mechanical flight control system and the automatic flight control system (AFCS). The AFCS includes the stability augmentation system (SAS), the pitch bias actuator, the flight-path stabilization (FPS), and an automatic stabilator. The FPS autopilot was not used in these simulations. Furthermore, the rotor rpm was assumed to be constant in this study, so that the engine dynamics and engine fuel controller were not modeled. An analytical definition of the control system is given in Ref. 29.

Because this model uses a blade-element rotor model, the effects of induced velocity as a result of the ship airwake can be easily achieved. Rotorcraft distributed inflow, downwash, and sidewash aerodynamics are affected by the ship airwake flowfield. However, it is assumed that the rotor wake does not in turn affect the ship airwake.

Gust Penetration Model

The gust penetration model is used to model the effects of a three-dimensional ship airwake. For the distribution of the gust velocities over the helicopter, the velocity field is determined at all of the distributed components on the helicopter. Thus the location of all of the components must be computed at each point in time relative to the ship. To account for local velocities at the rotor-blade elements, fuselage, empennage and tail rotor, a three-dimensional interpolation algorithm is applied. The ship airwake velocity field provided by the CFD database is defined with respect to a ship-fixed coordinate system. Thus, the velocity field must be transformed to inertial axes and then to the specific axis systems used for each of the helicopter component models. For the fuselage, empennage, and tail rotor, the following coordinate transformation is required:

$$\boldsymbol{V}_{\text{body}} = \boldsymbol{T}_{i2b}\boldsymbol{T}_{s2i}\boldsymbol{V}_{\text{ship}} \tag{1}$$

where $\boldsymbol{V}_{\text{ship}}$ is the ship wake velocity in ship coordinate system, $\boldsymbol{V}_{\text{body}}$ is the ship wake velocity in the helicopter body coordinate system, $\boldsymbol{T}_{s2i}$ is the coordinate transformation matrix from ship coordinate system to inertial coordinate system, and $\boldsymbol{T}_{i2b}$ is the coordinate transformation matrix from inertial to helicopter body coordinate system.

For each main rotor-blade element, a more complicated coordinate transformation is required:

$$\boldsymbol{V}_{\text{rotor}} = \boldsymbol{T}_{h2b}\boldsymbol{T}_{b2h}\boldsymbol{T}_{i2b}\boldsymbol{T}_{s2i}\boldsymbol{V}_{\text{ship}} \tag{2}$$

where $\boldsymbol{V}_{\text{rotor}}$ is the ship wake velocity in blade coordinate system, $\boldsymbol{T}_{b2h}$ is the coordinate transformation matrix from helicopter body

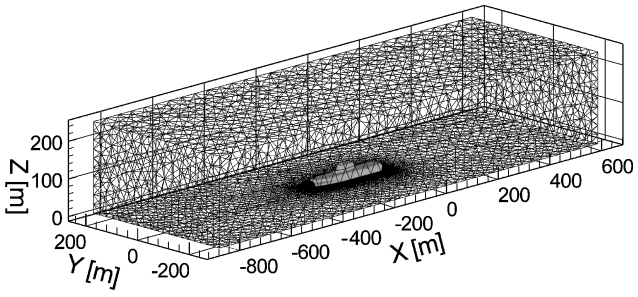

Fig. 4a Unstructured grid domain around the LHA.

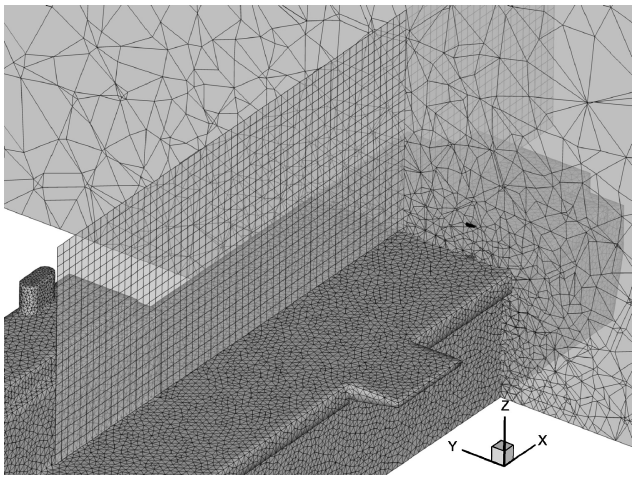

Fig. 4b Unstructured mesh on the ship surface and on a slice at $x = -27.432$ m.

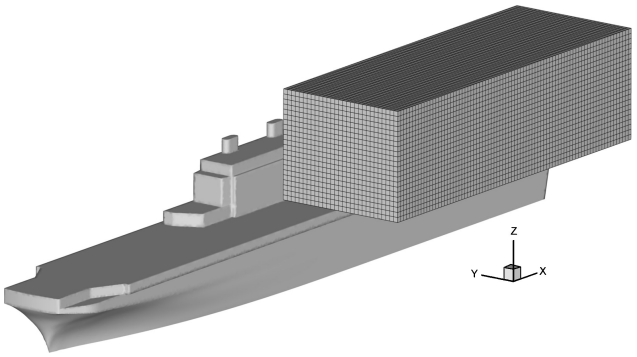

Fig. 5 Rectangular volumetric domain of CFD data at the rear deck of LHA for DI simulations.

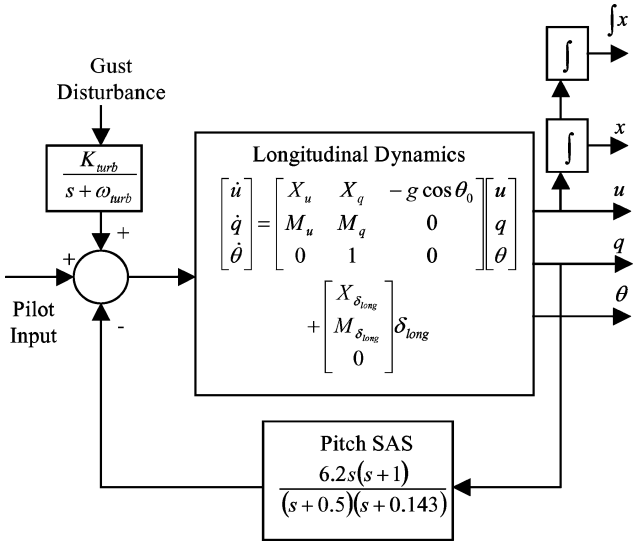

Fig. 2 Augmented plant model in longitudinal axis.

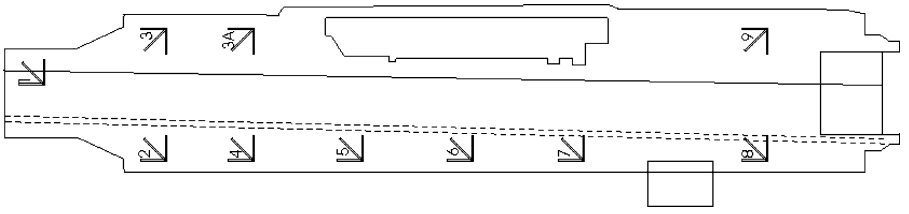

Fig. 3 Top view of LHA class ship.

to hub coordinate system, and $\boldsymbol{T}_{h2b}$ is the coordinate transformation matrix from hub to each blade coordinate system. These transformations must account for the orientation of the helicopter, the hub, and all of the rotor degrees of freedom.

The time-varying components of the airwake are stored at every 0.1 s for a total of 40 s of time history. Linear interpolation is used to calculate the gust field at every simulation time step (0.01 s). Because the maneuvers generally last longer than 40 s, the entire time-accurate flow solutions must be repeated. To prevent the sudden jump at every 40-s period, the solutions are overlapped with a sinusoidal filter for the first and last 5 s.

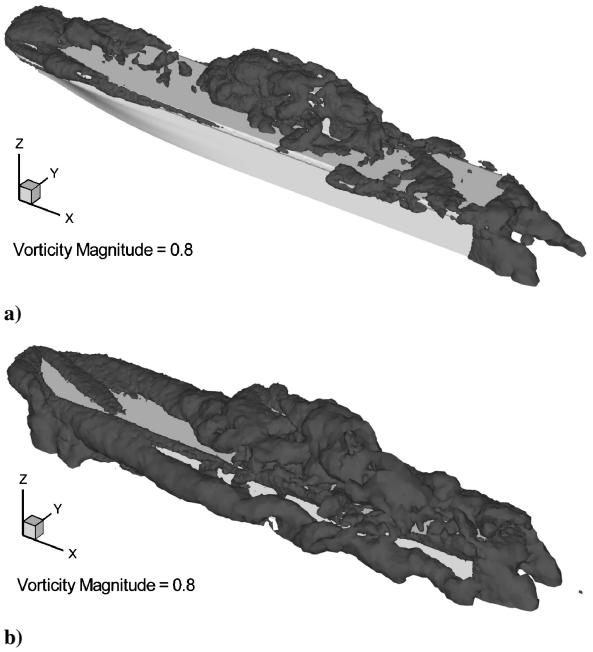

Fig. 6 Vorticity magnitude ($\sec^{-1}$) isosurface at $t = 40$ s for a) 0-deg WOD case and b) 30-deg WOD cases.

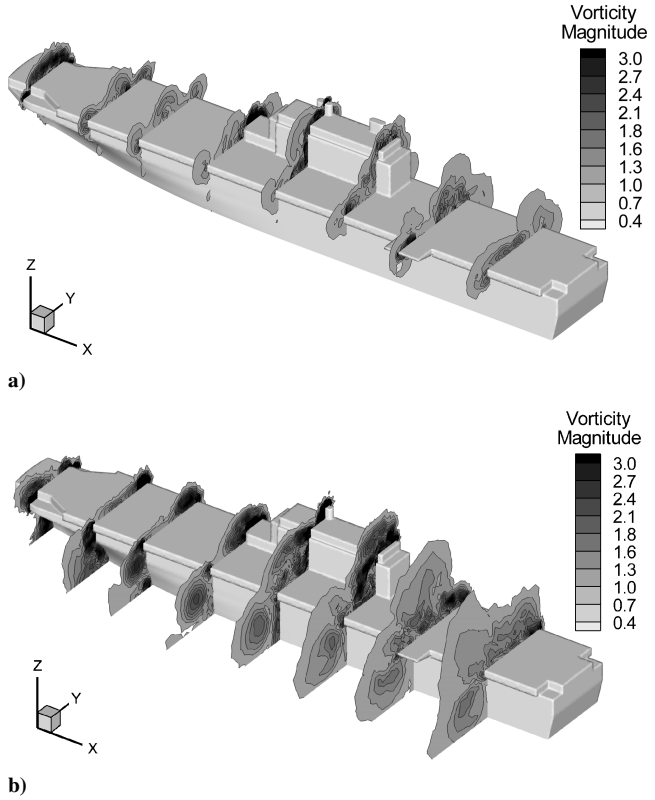

Fig. 7 Vorticity magnitude ($\sec^{-1}$) contours at $t = 40$ s at several stations along the ship for a) 0-deg WOD case and b) 30-deg WOD cases.

Optimal Control Model of a Human Pilot

Figure 1 represents a simplified optimal control model of a human pilot. In this study, the human pilot's basic task is to control the aircraft to follow the specified approach and departure trajectories. To design an optimal control model of a human pilot, the aircraft is represented with linearized equations of motion in state variable form:

$$\dot{\boldsymbol{x}}(t) = \boldsymbol{A}\boldsymbol{x}(t) + \boldsymbol{B}\boldsymbol{u}(t) + \boldsymbol{w}(t), \qquad \boldsymbol{y}(t) = \boldsymbol{C}\boldsymbol{x}(t) + \boldsymbol{v}(t) \quad (3)$$

where $\boldsymbol{x}(t)$ is the state vector, $\boldsymbol{u}(t)$ is the pilot's control input vector, $\boldsymbol{w}(t)$ is a vector of external disturbances, $\boldsymbol{y}(t)$ is vector of measurements (parameters perceived by the pilot), and $\boldsymbol{v}(t)$ represents observation noise. The human pilot model in Fig. 1 is represented as an optimal linear regulator in combination with an optimal state estimator (Kalman estimator). Both the estimator and feedback gain matrix are determined by solving the linear quadratic Gaussian control problem. Assuming the linear dynamics of Eq. (3) and the disturbance are white-noise signals, the objective is to find a dynamic compensator that minimizes the quadratic performance index given by

$$J = E\left\{ \lim_{T\to\infty} \frac{1}{T} \int_0^T [\boldsymbol{x}^T(t)\boldsymbol{Q}\boldsymbol{x}(t) + \dot{\boldsymbol{u}}(t)\boldsymbol{R}\dot{\boldsymbol{u}}(t)]\,\mathrm{d}t \right\} \quad (4)$$

where $\boldsymbol{Q}$ and $\boldsymbol{R}$ are the state and control weighting matrices. The estimator and feedback gains are readily solved from a pair of matrix Riccati equations. When modeling human operators, it is customary

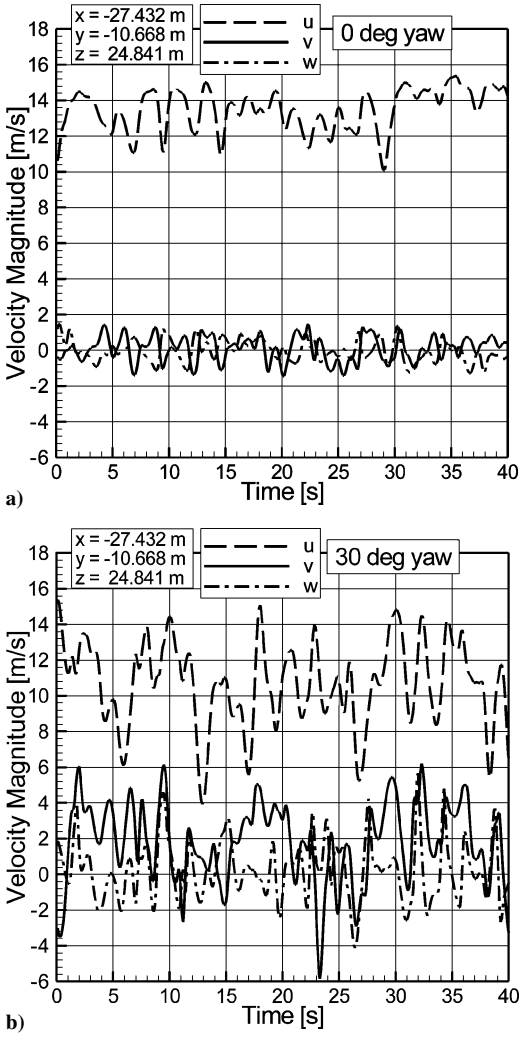

Fig. 8 Time histories of velocity components (u, v, w) of CFD data at a selected point in the DI mesh for a) 0-deg WOD and b) 30-deg WOD cases.

to use control rates instead of the control position in the performance index. A simple augmentation of the plant dynamics model is used to achieve this.[26] Details of the complete optimal control model of the human operator are discussed in Refs. 24 and 26.

A numerical linearization of the simulation model is used to obtain a 24-state model, which includes nine rigid-body states and 15 states associated with rotor dynamics and inflow. For this study, the model was linearized about a hover equilibrium in a 30-kn wind (which represents the terminal phase of the approach maneuver). Assuming quasi-static rotor and inflow dynamics, the linear model is reduced to a nine-state/six-DOF model of the rigid-body motion. The linear model is decoupled into a three-state longitudinal model, a five-state lateral-directional model, and a one-state vertical motion model. Finally, the linear models must be augmented to include shaping filters for the gust disturbances and a dynamic model of the SAS for each axis. Integrators are added so that position and integrated position can be included in the performance index. A schematic of the augmented flight dynamics model used for longitudinal control is shown in Fig. 2. A similar model was used for lateral-directional control, which includes pilot inputs in both the lateral and directional axes.

A key task in developing an appropriate optimal control model of the human pilot is the selection of the appropriate weighting matrices $\boldsymbol{Q}$ and $\boldsymbol{R}$. The effect of the parameter weighting parameters is not as clear as in the case of the crossover model of the human operator because the optimal control model parameters are essentially inputs to an optimization scheme that involves the solution of sets of nonlinear algebraic equations.[24] However, Ref. 26 outlines an approximate method for selecting these parameters to achieve a desired crossover frequency for each control axis.

Typically, both the $\boldsymbol{Q}$ and $\boldsymbol{R}$ matrices are assumed to be diagonal. The weighting parameters in the $\boldsymbol{Q}$ matrix are selected such that each state variable is scaled by its maximum expected deviation.[26] This leaves the task of selecting the control weighting parameters in $\boldsymbol{R}$. Consider the longitudinal axis where the transfer function from longitudinal control input to pitch attitude can be expressed as

$$\frac{\theta}{\delta_{\text{long}}}(s) = \frac{K\left(s^m + a_{m-1}s^{m-1} + \cdots + a_1 s + a_0\right)}{\left(s^n + b_{n-1}s^{n-1} + \cdots + b_1 s + b_0\right)} \tag{5}$$

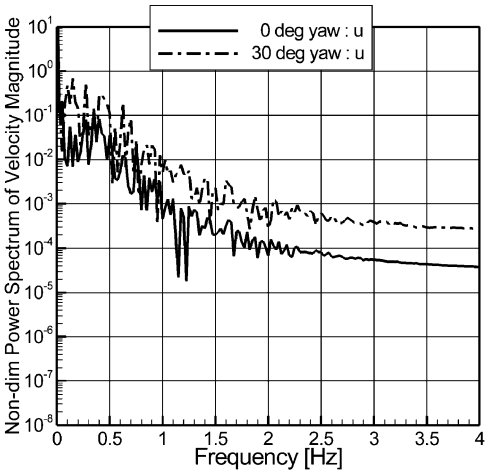

a) *u*- velocity component

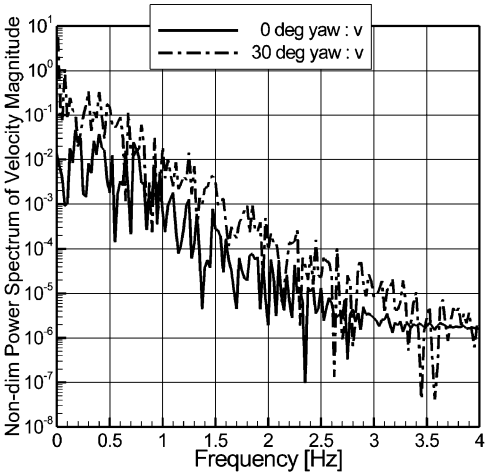

b) *v*-velocity component

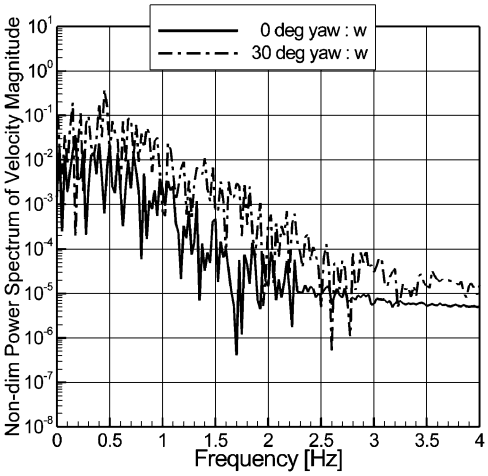

c) *w*-velocity component

Fig. 9 Nondimensional power spectrum of velocity components at a selected point in the DI mesh over landing spot 8 for 0- and 30-deg WOD cases.

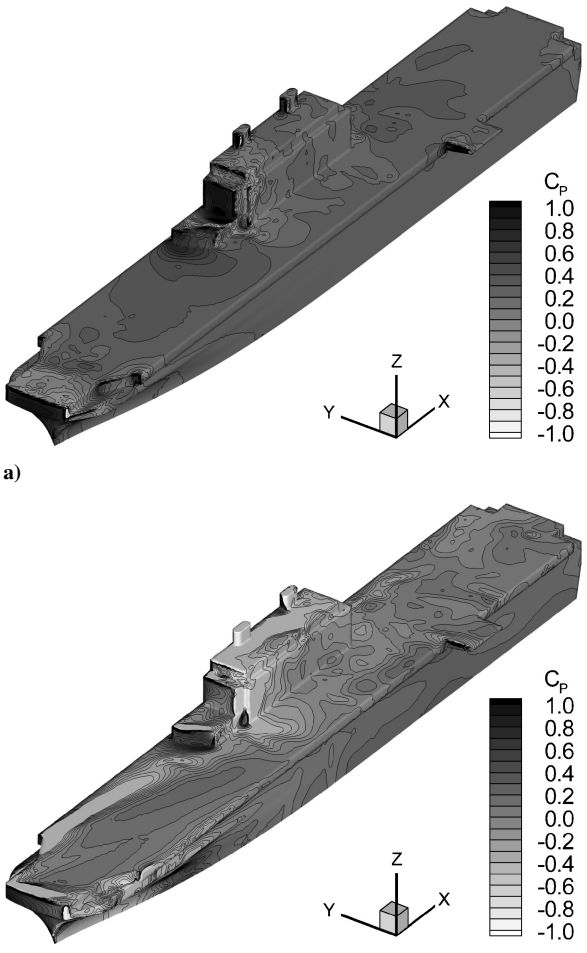

a)

b)

Fig. 10 Pressure coefficient contours on the ship surface at $t = 40$ s for a) 0-deg and b) 30-deg WOD cases.

An approximate but very useful relationship exists between the weighting coefficients, the controlled-element dynamics, and the closed-loop system bandwidth[24,26]:

$$\omega_{\mathrm{BW}} \approx \left[K \left(q_\theta / r_{\delta_{\mathrm{long}}} \right)^{\frac{1}{2}} \right]^{1/(n-m+1)} \tag{6}$$

where q_θ is the weighting parameter for pitch attitude, $r_{\delta_{\mathrm{long}}}$ is the longitudinal control weighting, and ω_{BW} is closed-loop bandwidth (frequency where the amplitude of the closed-loop transfer function is 6 dB below its zero-frequency value). The following is an approximate relation between the open-loop crossover frequency and the closed-loop bandwidth:

$$\omega_c \approx 0.56 \omega_{\mathrm{BW}} \tag{7}$$

Thus, given a desired crossover frequency in each control axis, Eqs. (5–7) provide a method of determining appropriate control weighting parameters in $\boldsymbol{R}$. In addition, the pilot model can be designed so that the tracking performance can be easily tuned based on a desired crossover frequency in each control axis.

In this study, the desired crossover frequencies were set to 1.25 rad/s for the longitudinal axis and 1.75 rad/s for the lateral and directional axes. As Eqs. (5–7) are approximations, they result in crossover frequencies that differ slightly from the desired crossover frequency specified in the OCM design. However, using Eq. (7) as an initial guess the weighing parameters in R were changed iteratively so that the differences between the actual and desired crossover frequencies were less than 0.5%. The iteration process was automated in MATLAB and was found to converge in a nominal amount of processor time. The objective of this study was to develop a pilot model that can be easily tuned based on expected crossover frequencies in each control axis. The crossover frequencies used in this study are reasonable values for a human pilot, but more exact values might be derived from flight-test data.

Figure 1 also includes blocks labeled neuromotor dynamics and time delay. These terms can be used to account for the physiological limitations on the ability of human pilots to make corrective actions. In this study a time constant $\tau_n = 0.1$ s was used, and the time delay was set to 0.1 s. These are typical values used in modeling human performance.[24]

Control records from human helicopter pilots have shown that there is a stepped appearance in the collective control input.[25] Pilots tend to make discrete rather than continuous adjustments to the collective lever. This effect can be modeled using nonlinear elements (hysteresis and deadband) in the pilot model.[25] The hysteresis element represents a system in which a change in input causes an equal change in output. However, when the input changes direction an initial change in input has no effect on the output. The amount of

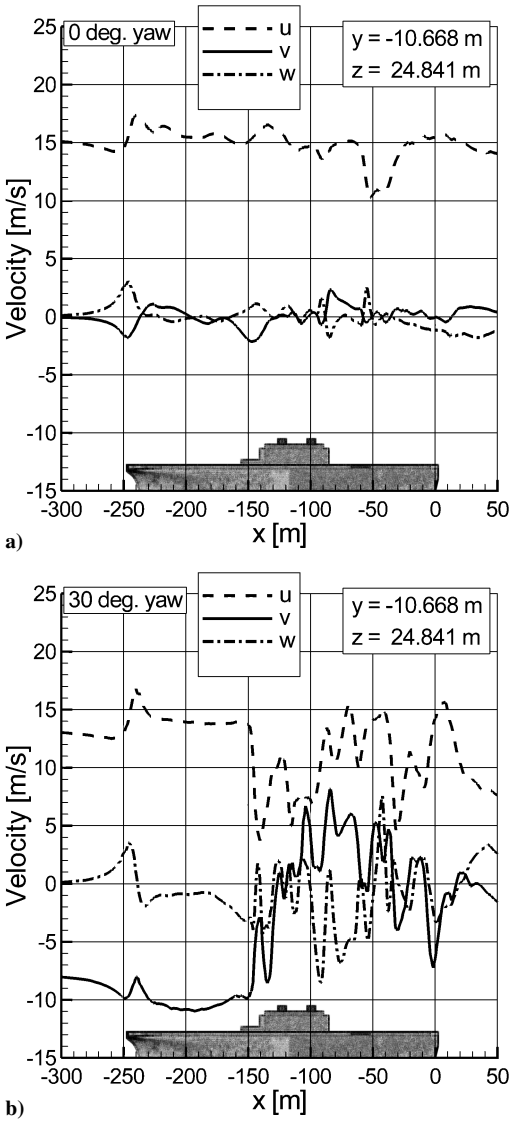

Fig. 11 Distribution of the velocity components along the ship on a *xz* plane crossing the landing spot 8 and 17 ft above the deck at $t = 40$ s for a) 0-deg and b) 30-deg WOD cases.

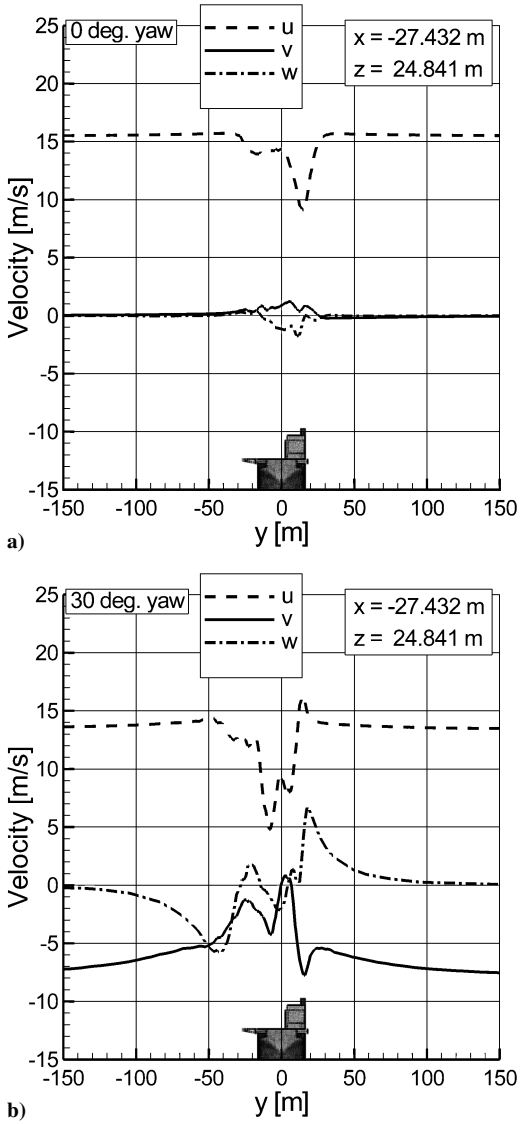

Fig. 12 Distribution of the velocity components across the ship on a *yz* plane crossing the landing spot 8 and 17 ft above the deck at $t = 40$ s for a) 0-deg and b) 30-deg WOD cases.

side-to-side play in the system is referred to as the deadzone. The deadband element represents a threshold of perception of departure from the desired trajectory. Therefore, the deadband generates zero output within a specified region. These nonlinear elements are incorporated only with collective control.

Shipboard Operations

In this study, typical shipboard approach and departure trajectories are simulated. Kinematic profiles of these shipboard tasks are given in Ref. 23, and these profiles are modified slightly in this study. As discussed in Ref. 23, the kinematic profile is determined using an Earth-fixed coordinate frame with the origin at the sea surface directly under the initial position of the helicopter. The *X* axis is along with the North direction, *Z* axis is downward, and *Y* axis is along with the East direction. The target spot of shipboard operations is spot 8 of the LHA class ship (Fig. 3).

Typical shipboard approach procedures include all actions that bring the rotorcraft from a point far away from the ship down to a point much closer to the recovery spot.[19,23] The key parameters for defining the approach profile are the helicopter initial level flight speed, initial altitude, initial distance from the ship, and desired final altitude for stationkeeping. In this study, it is assumed that the helicopter approaches the ship from the port side at a 45-deg angle and then performs a 45-deg left turn to align itself with the longitudinal axis of the ship after it crosses over the deck. This is similar to the trajectory used in the JSHIP study.

Similarly, typical shipboard departure procedures include all actions that are required to conduct an ascending, acceleration from stationkeeping, ending in steady, level forward flight.[19,23] Starting from the stationkeeping location, pilots typically initiate the departure phase by yawing and/or translating the helicopter at a relatively constant altitude to a position outboard of the recovery spot that

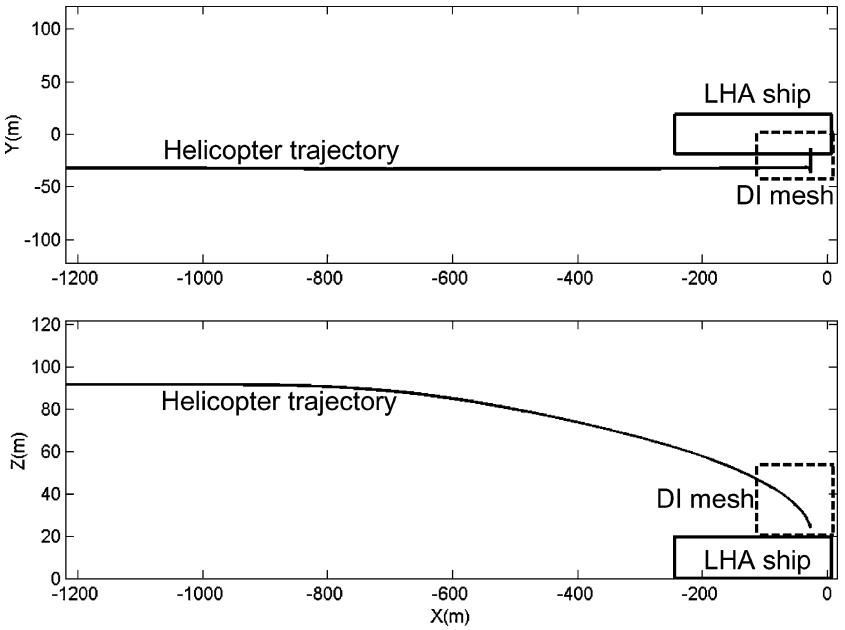

Fig. 13 Helicopter position (m) with respect to ship coordinate system—departure case (30 deg).

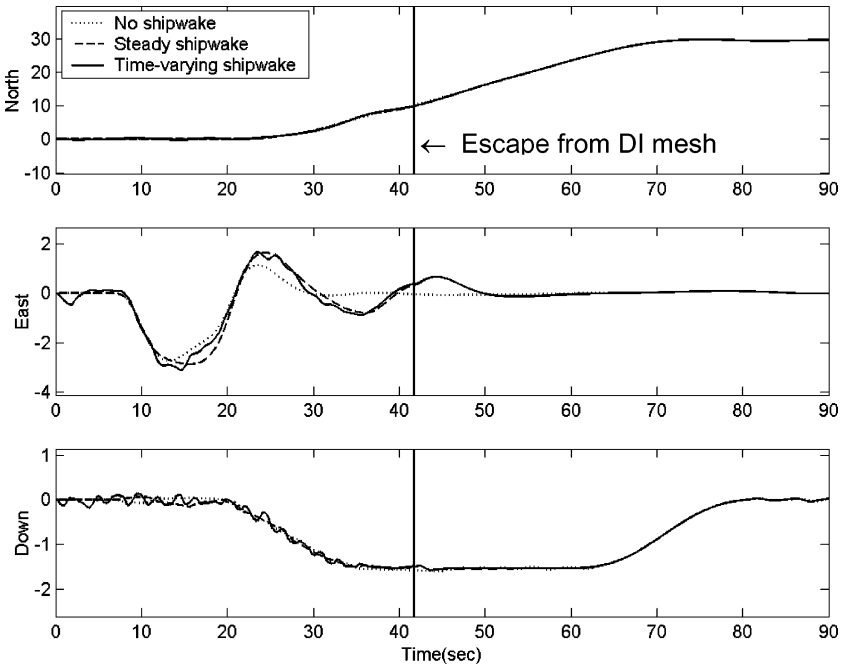

Fig. 14 Helicopter velocity (m/s) vs time—departure case (30 deg).

is clear of obstructions. The helicopter then transitions to a desired climb rate and horizontal acceleration. Finally, the helicopter achieves desired level flight speed.

Simulation Results

CFD Simulation of Ship Airwake

In this study, the simulation model is interfaced with steady-state and time-accurate inviscid CFD predictions for an LHA ship airwake. Figure 4a shows the three-dimensional unstructured grid for the full-scale LHA geometry, which is generated using the GRIDGEN software. The rectangular computational grid has 854,072 cells. The unstructured mesh on the ship surface is shown in Fig. 4b. The location of the spot 8, which is considered in this paper for a target spot of shipboard operations, is also illustrated in this figure by a cutting yz plane crossing this spot and a circular mark centered 5.182 m (17 ft) above the deck on this plane over the spot.

The flow case represents both 0- and 30-deg yaw angles and 15.433 m/s (30 kn) of relative wind speed. These are the same cases simulated by Polsky and Bruner.[15] A four-stage Runge–Kutta explicit time-integration algorithm with Roe's flux-difference scheme is used with Courant–Friedrichs–Lewy numbers of 2.5 and 0.8 for the steady and unsteady computations, respectively.

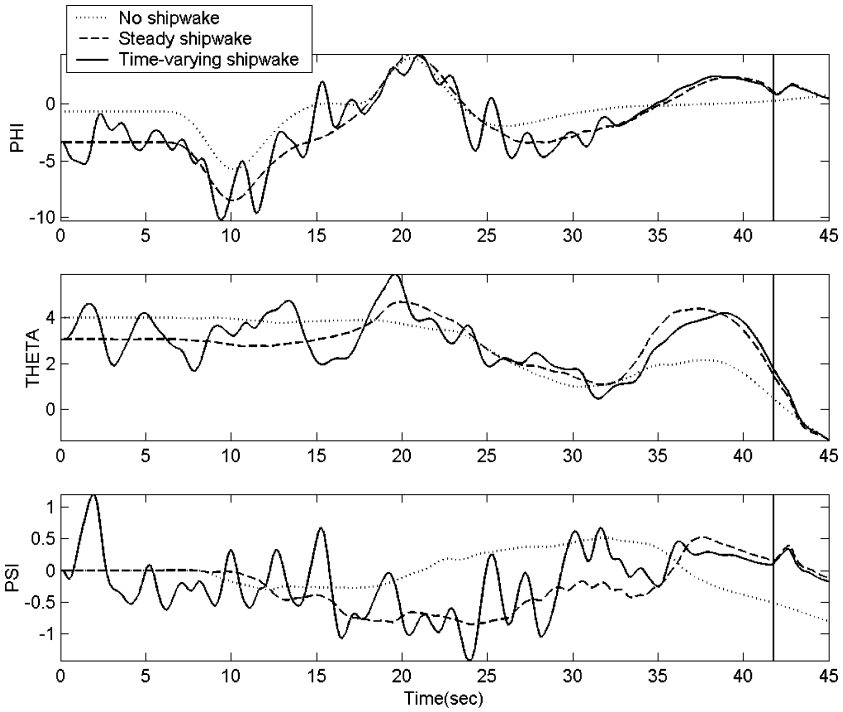

Fig. 15 Helicopter attitude (deg) in the DI mesh—departure case (30 deg).

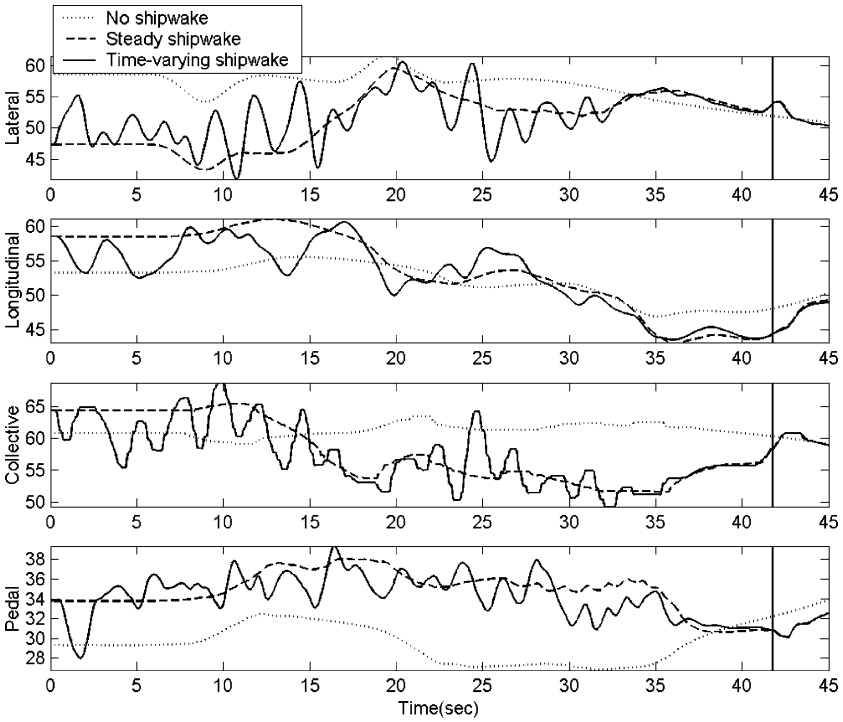

Fig. 16 Pilot inputs (%) in the DI mesh—departure case (30 deg).

A zero-normal-velocity boundary condition is applied on the ship surface and water surface (bottom surface of the domain), and a Riemann boundary condition is applied at all other faces of the domain. The pseudo-steady-state computations are performed using local time stepping and initialized with freestream values. The time-accurate computations are started from the pseudo-steady-state solution, and the simulation time step (480 μs) is determined by the smallest cell size in the volume grid. The computations are performed on a parallel PC cluster Lion-XL consisting of 256 2.4-Ghz P4 processors with 4-GB ECC RAM and Quadrics high-speed interconnect. It takes nearly 2080 iterations to simulate 1 s of real flow ($\sim$1.8 h on 12 processors) with the current grid.

The time-accurate CFD solutions result in large quantities of time history data that need to be mapped into the DI simulation gust penetration model. Thus, for a given launch or recovery operation the velocity data can be mapped into a rectangular grid (to allow easy table look up) and stored for only that part of the ship where the aircraft is expected to fly. Figure 5 shows the rectangular volumetric domain of CFD data over the rear deck of LHA for DI simulations. This DI mesh has ($81 \times 30 \times 23$) grid points with 1.524-m (5-ft) equal intervals, and it is selected to have the flow data over landing spots 7 and 8. The helicopter enters the DI mesh from the back surface and escapes from it through the front surface according to the calculated approach and departure trajectories. A total of 50 s

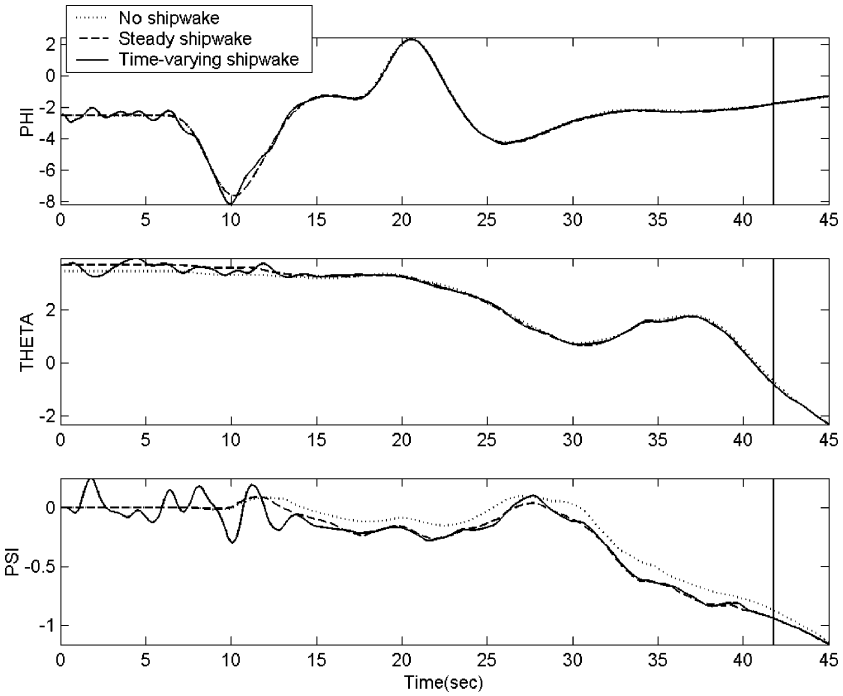

Fig. 17 Helicopter attitude (deg) in the DI mesh—departure case (0 deg).

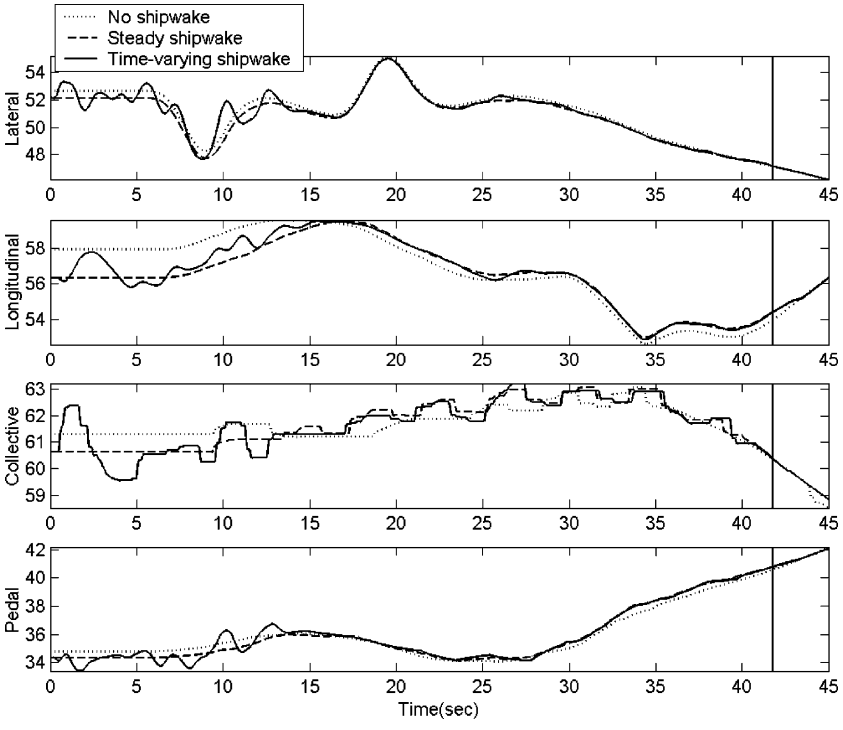

Fig. 18 Pilot inputs (%) in the DI mesh—departure case (0 deg).

of time-accurate flow solution is obtained. Only the last 40 s of the time-history data are stored for every 0.1 s to be used for the DI simulations. Each flow solution file is 41 Mbytes in size, whereas a DI velocity data file is only 5.2 Mbytes.

Isosurfaces of vorticity magnitude of 0.8 s^{-1} for both 0- and 30-deg WOD cases are shown in Fig. 6. The vorticity magnitude contours at $t = 40$ s at several stations corresponding to different landing spots along the ship are shown in Fig. 7 for both WOD cases. Similar features can be observed as in Ref. 2 such as bow separation, deck-edge vortices, complex island wake for both cases, and burbles in the flowfield between the bow separation and the island for the zero-yaw case. For the 30-deg WOD case, more complex island wake can be observed especially over the landing spots 7 and 8. Figure 8 shows time histories of velocity components (u, v, w) of CFD data at a selected point (5.182 m above the deck) in the DI mesh over landing spot 8 for 0- and 30-deg yaw cases. The velocity data at that point, which is located at (−27.432 m, −10.668 m, 24.8412 m) (−90 ft, −35 ft, 81.5 ft), are extracted from the 40 s of real flow solutions with 0.1 s of intervals. The power spectrum of the velocity components, nondimensionalized by the square of the freestream velocity, vs frequency is plotted in Fig. 9. The power spectra of the 30-deg yaw case generally have higher amplitude than those of the 0-deg yaw case. This is probably because of the larger and stronger vortical structures present in the wake. For the 30-deg case, there is strong unsteadiness in the crossflow (y component) and vertical (z component) components of the velocity over this spot. Also, the fluctuations in the velocity components are much higher than those in 0-deg yaw case.

Pressure coefficient contours on the ship surface at $t = 40$ s in Fig. 10 also show the major differences of flow features between both 0- and 30-deg yaw cases. Low-pressure areas correspond to the separated flow regions. Flowfield differences between the two

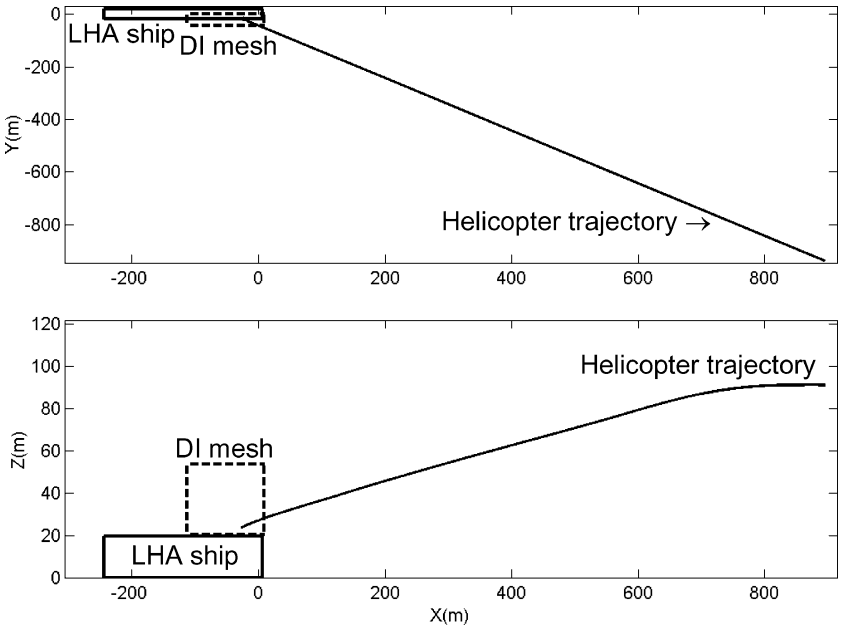

Fig. 19 Helicopter position (m) with respect to ship coordinate system—approach case (30 deg).

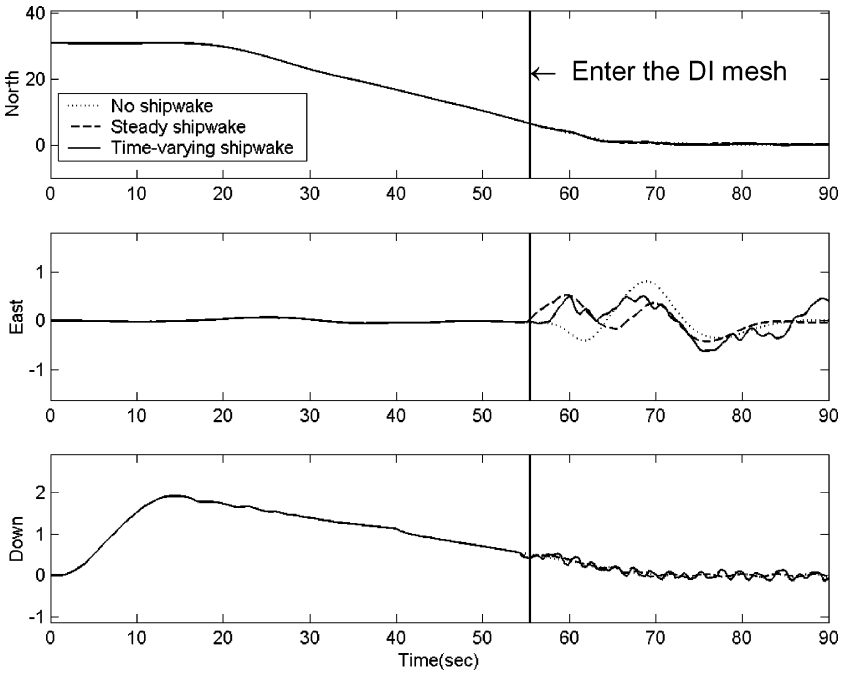

Fig. 20 Helicopter velocity (m/s) vs time—approach case (30 deg).

WOD cases and the complexity of the flow over the ship deck can also be observed by the distribution of the instantaneous velocity components along and across the ship at the selected point 5.182 m (17 ft) above the landing spot 8 in Figs. 11 and 12.

Dynamic Interface Simulation Results

The dynamic interface flight dynamics model has been applied to simulate the UH-60 operating near an LHA class ship. In this study, the helicopter/ship dynamic interface simulation has been performed for three different airwake cases (no airwake, steady-state airwake, time-varying airwake) in 0- and 30-deg WOD conditions. The optimal control model was used to determine the required pilot control inputs for shipboard approach and departure tasks. For both departure and approach operations, the ship is assumed to be still with a steady-state wind of 30 kn. For the departure case, to clear obstructions the departure begins with a 18.29-m (60-ft) translational maneuver to the left (port side). The general profile parameters of the shipboard departure are shown in Table 1.

Figures 13–18 show the simulation results for departure operation in 0- and 30-deg WOD cases. The dotted lines represent the no-airwake condition, the dashed lines represent the steady airwake condition, and the solid lines represent the time-varying airwake

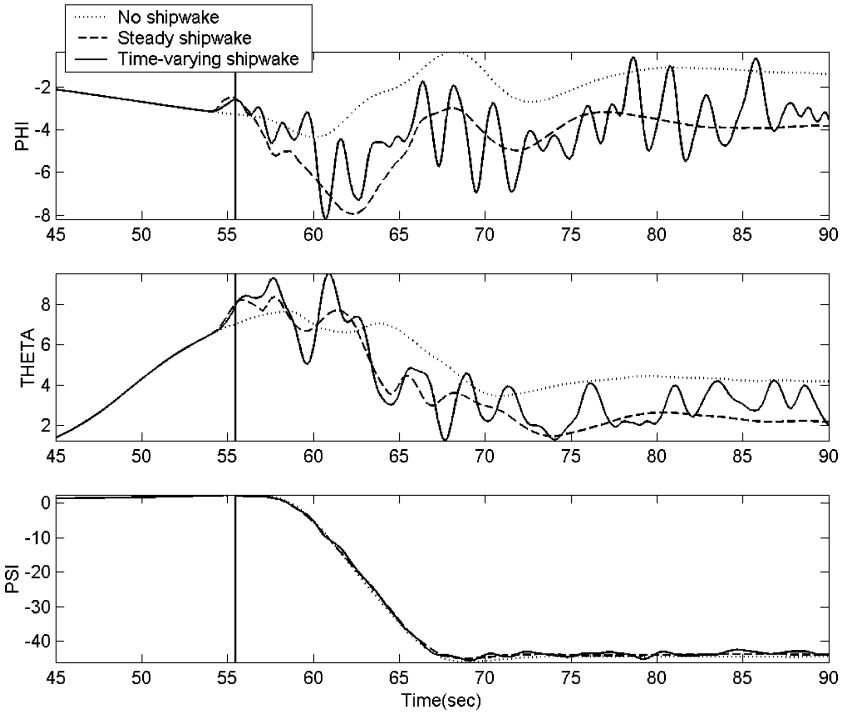

Fig. 21 Helicopter attitude angle (deg) after entering the DI mesh—approach case (30 deg).

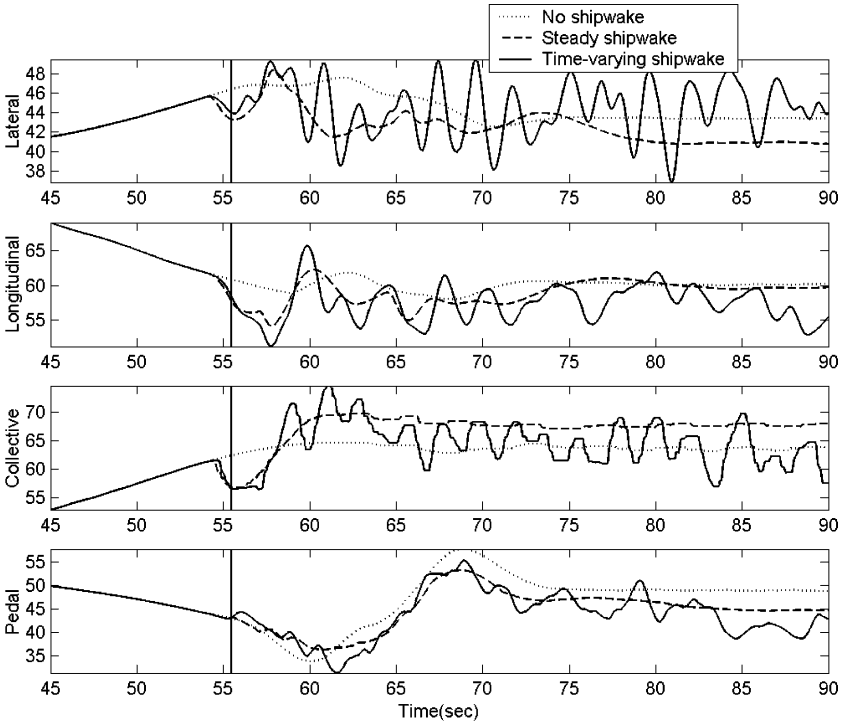

Fig. 22 Pilot inputs (%) after entering the DI mesh—approach case (30 deg).

Table 1 Initial profile parameters for shipboard operations

Trajectory parameters	Approach	Departure
Initial altitude	91.44 m (300 ft)	24.384 m (80 ft) −5.182 m (17 ft) above deck-
Final altitude	24.384 m (80 ft)	91.44 m (300 ft)
Initial speed	30.867 m/s (60 kn)	0 kn
Final speed	0 kn	30.867 m/s (60 kn)

condition. The helicopter trajectory with respect to the ship coordinate system is shown in Fig. 13. Figure 14 shows the helicopter velocity in North-East-Down (NED) coordinate system. Figure 15 shows the helicopter attitude responses. The pilot stick inputs provided by the optimal control model are shown in Fig. 16. The conventions for these control positions are as follows: full left lateral cyclic, full forward longitudinal cyclic, full down collective pitch, and full left pedal correspond to 0%, full right lateral cyclic, full aft longitudinal cyclic, full up collective pitch, and full right pedal

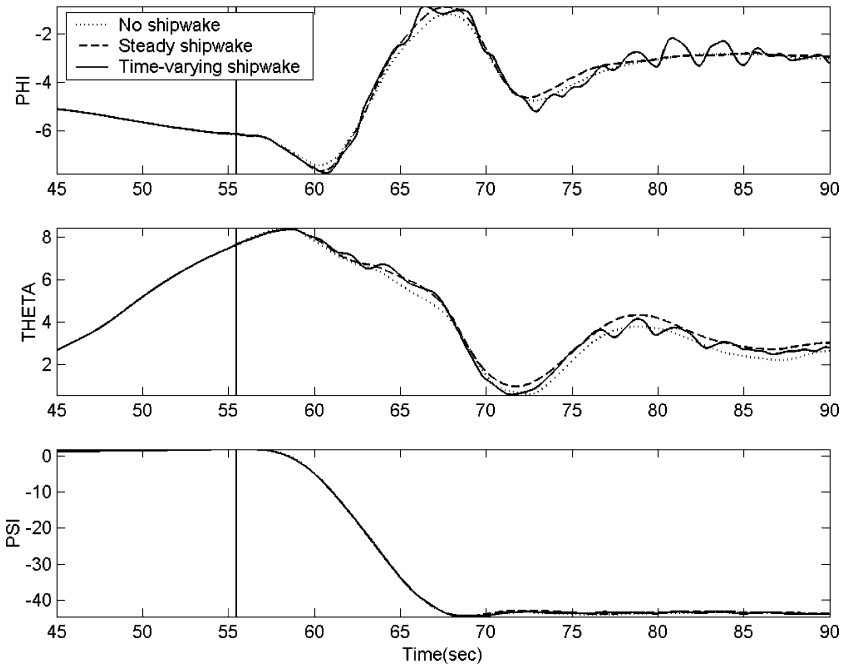

Fig. 23 Helicopter attitude (deg) after entering the DI mesh—approach case (0 deg).

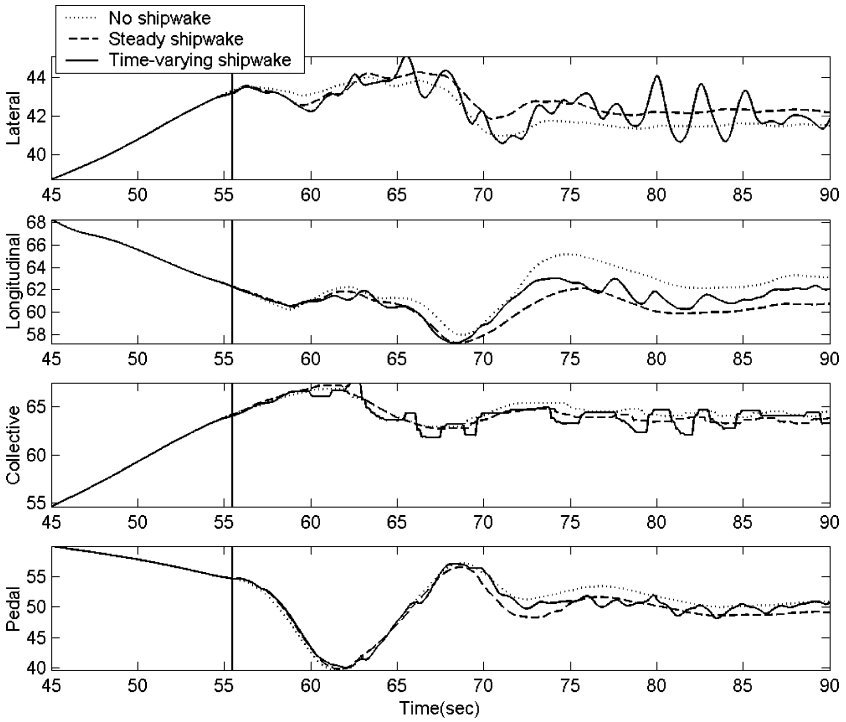

Fig. 24 Pilot inputs (%) after entering the DI mesh—approach case (0 deg).

correspond to 100%. The results show that the helicopter trajectory and velocities are very similar in each case. This is because the optimal control model of the human pilot is regulating these parameters. These variables are essentially constrained in the simulation; the optimal control model is effectively calculating the control inputs and aircraft attitude required to track the desired trajectory. However, when the helicopter is operating within the DI mesh there is significant difference in the aircraft attitude response and the pilot control activity. The steady airwake results differ only slightly from the results with no airwake in that the trimmed controls and attitude are different. However, the time-varying airwake results in significant oscillations and pilot activity, particularly when hovering over the ship deck. This difference in the results with the steady and time-varying airwake was not entirely expected because a stationary gust field can appear to be time varying to the aircraft when it is moving (and especially to the rotor blades, which are constantly moving). As discussed in the preceding section, there is strong unsteadiness in the crossflow (y component) and vertical (z component) components of the velocity caused by bow separation, deck-edge vortices, and complex island wake for 30-deg WOD condition. These effects can be clearly observed from results of aircraft attitude responses and pilot control activities (Figs. 15–18). Note that the differences in the beginning are caused by the different trim conditions. From the results, the 30-deg WOD condition results in significantly larger oscillations and higher pilot control activity, particularly when hovering over the ship deck. This is consistent with the JHSIP flight-test data.[19,20]

Figures 19–24 show similar simulation results for the approach operation. As expected, the attitude changes and control activity are fairly benign in the early part of the maneuver, when the helicopter is relatively far from the ship. Near the end of the maneuver, the helicopter begins to interact significantly with the time-varying airwake, as indicated by the fluctuations in attitude and increased control activity. It can also be observed that the oscillations immediately after entering the DI mesh are similar for the steady and time-varying airwake. At this point, the aircraft is still moving with significant velocity so that the steady gust field has a time-varying appearance to the aircraft. However, once the aircraft approaches hover the results indicate the time-varying airwake results in larger oscillations and higher pilot control activity than the steady airwake. This reflects the so-called cliff edge effect,[18] where strong shear layers from the ship's superstructure are blown across the landing spot with winds from 30 deg.

For both operations, compared to the case with no airwake, the trim conditions of the helicopter with the ship airwake are different (in terms of pilot control inputs and helicopter attitude). These differences are clearly induced as a result of the ship airwake. From the results, the optimal control model is reasonably effective in tracking the desired flight path for both approach and departure operations. It is quite apparent that the time-varying ship airwake is very significant for helicopter/ship dynamic interface testing. These ship airwake effects can increase pilot workload and possibly degrade handling qualities during shipboard launch and recovery operations.

Conclusions

A helicopter/ship dynamic interface simulation tool has been developed to model a UH-60A operating off an LHA class ship. To achieve a high-fidelity simulation model, time-accurate ship airwake solutions of an LHA class ship are integrated with the flight dynamics simulation model. These ship airwake solutions are calculated using the flow solver PUMA2. Both steady-state and time-accurate inviscid ship airwake flowfields are calculated for the three-dimensional full-scale LHA geometry. Approach and departure trajectories were simulated from landing spot 8 on the LHA [computational-fluid-dynamics (CFD) results showed significant time-varying flow effects over this spot]. Results with no ship airwake, steady airwake, and time-varying airwake were compared. Although continued research is recommended to prove the capability of the simulation tool developed in this study, a fundamental simulation testing tool has been developed to provide insight into the helicopter/ship dynamic interface problem. Based on the results presented in this paper, the following conclusions can be made:

1) The results clearly indicate that the time-varying airwake has a significant impact on aircraft response and pilot control activity when the aircraft is flown for specified approach and departure trajectories. The differences are most notable when the helicopter is operating in or near a hover relative to the ship deck (stationkeeping). In the past, gust models for fixed-wing aircraft simulation have often used a stationary or frozen field model. This is adequate when the aircraft is moving at a significant forward speed. However, the model clearly breaks down as airspeed approaches zero. The same appears to be true of helicopters operating in turbulent ship airwake. The time-varying nature of the ship airwake becomes dominant as the helicopter approaches hover. And, the 30-deg WOD condition showed a substantial increase in pilot workload.

2) An optimal control model of the human pilot was successfully implemented to solve the inverse simulation problem. Given a specified trajectory, the pilot controls can be calculated using forward simulation in conjunction with a feedback controller. This was found to be highly useful for this research task. Inverse simulations can be time consuming and difficult to implement computationally. The pilot model was easily tuned and seemed to produce reasonable predictions of trajectory tracking and pilot control activity.

3) The use of time-accurate ship airwake data was found to present some practical implementation difficulties, in that the method requires that the simulation handle large quantities of data. For every grid point a set of time-history data must be stored for each component of velocity. Memory storage can become an issue, particularly if the simulations are to be run in real time, in which case accessing data from disk storage might not be feasible. It was helpful to select a subset of the flowfield when performing the simulations in which the landing spot is known. However, for real-time simulations the pilot might want to access different deck spots during the same simulation run. The use of stochastic airwake model (based on the time-accurate CFD results) might be an attractive alternative.

References

[1]Mello, O. A. F., Prasad, J. V. R., Sankar, L. N., and Tseng, T., "Analysis of Helicopter/Ship Aerodynamic interactions," *Proceedings of the American Helicopter Society Aeromechanics Specialists Conference*, American Helicopter Society, Alexandria, VA, 1994, pp. 6.5-1–6.5.7.

[2]Polsky, S. A., "A Computational Study of Unsteady Ship Airwake," AIAA Paper 2002-1022, Jan. 2002.

[3]Daley, W. H., "Flow Visualization of the Airwake Around a Model of a TARAWA Class LHA in a Simulated Atmospheric Boundary Layer," M.S. Thesis, Dept. of Aeronautical Engineering, Naval Postgraduate School, Monterey, CA, June 1988.

[4]Johns, M. K., "Flow Visualization of the Airwake Around a Model of a DD-963 Class Destroyer in a Simulated Atmospheric Boundary Layer," M.S. Thesis, Dept. of Aeronautical Engineering, Naval Postgraduate School, Monterey, CA, Sept. 1988.

[5]Rhodes, M. M., and Healey, J .V., "Flight Deck Aerodynamics of a Nonaviation Ship," *Journal of Aircraft*, Vol. 29, No. 4, 1992, pp. 619–626.

[6]Zan, S. J., and Garry, E. A., "Wind Tunnel Measurements of the Airwake Behind a Model of a Generic Frigate," NRC-CNRC Rept. LTR-AA-13, Ottawa, June 1994.

[7]Zan, S. J., Syms, G. F., and Cheney, B. T., "Analysis of Patrol Frigate Air Wakes," *Proceedings of the NATO RTO Symposium on Fluid Dynamics Problems of Vehicles Operating near or in the Air-Sea Interface*, Amsterdam, 1998.

[8]Cheney, B. T., and Zan, S. J., "CFD Code Validation Data and Flow Topology for The Technical Co-Operation Program AER-TP2 Simple Frigate Shape," National Research Council Canada Inst. for Aerospace Research, NRC-CNRC Report LTR-A-035, Ottawa, April 1999.

[9]Tai, T. C., "Simulation and Analysis of LHD Ship Airwake by Navier–Stokes Method," *Proceedings of the NATO RTO Symposium on Fluid Dynamics Problems of Vehicles Operating near or in the Air-Sea Interface*, Amsterdam, 1998.

[10]Tattersall, P., Albone, C. M., Soliman, M. M., and Allen, C. B., "Prediction of Ship Air Wakes over Flight Decks Using CFD," AGARD, Paper No. 6, Oct. 1998.

[11]Liu, J., and Long, L. N., "Higher Order Accurate Ship Airwake Predictions for the Helicopter-Ship Interface Problem," *Proceedings of the 54th*

American Helicopter Society Annual Forum, American Helicopter Society, Alexandria, VA, May 1998, pp. 58–70.

[12]Guillot, M. J., and Walker, M. A., "Unsteady Analysis of the Air Wake over the LPD-17," AIAA Paper 2000-4125, Aug. 2000.

[13]Reddy, K. R., Toffoletto, R., and Jones, K. R. W., "Numerical Simulation of Ship Airwake," *Computers and Fluids*, Vol. 29, No. 4, 2000, pp. 451–465.

[14]Sharma, A., and Long, L. N., "Airwake Simulations on an LPD 17 Ship," AIAA Paper 2001-2589, June 2001.

[15]Polsky, S. A., and Bruner, C. W. S., "Time-Accurate Computational Simulations of an LHA Ship Airwake," AIAA Paper 2000-4126, Aug. 2000.

[16]Bogstad, M. C., Habashi, W. G., Akel, I., Ait-Ali-Yahia, D., Giannias, N., and Longo, V., "Computational-Fluid-Dynamics Based Advanced Ship-Airwake Database for Helicopter Flight Simulators," *Journal of Aircraft*, Vol. 39, No. 5, 2002, pp. 830–838.

[17]Zan, S. J., "Computational-Fluid-Dynamics Based Advanced Ship-Airwake Database for Helicopter Flight Simulation," *Journal of Aircraft*, Vol. 40, No. 5, 2003, p. 1007.

[18]Camelli, F. E., Soto, O., Lohner, R., Sandberg, W. C., and Ramamurti, R., "Topside LPD17 Flow and Temperature Study with an Implicit Monolithic Scheme," AIAA Paper 2003-0969, Jan. 2003.

[19]Roscoe, M. F., and Wilkinson, C. H., "DIMSS—JSHIP's Modeling and Simulation Process for Ship/Helicopter Testing and Training," AIAA Paper 2002-4597, Aug. 2002.

[20]Wilkinson, C. H., Roscoe, M. F., and VanderVliet, G. M., "Determining Fidelity Standards for the Shipboard Launch and Recovery Task," AIAA Paper 2001-4062, Aug. 2001.

[21]Roscoe, M. F., Wilkinson, C. H., and VanderVliet, G. M., "The Use of ADS-33D Useable Cue Environment Techniques for Defining Minimum Visual Fidelity Requirements," AIAA Paper 2001-4063, Aug. 2001.

[22]He, C., Kang, H., Carico, D., and Long, K., "Development of a Modeling and Simulation Tool for Rotorcraft/Ship Dynamic Interface Testing," *Proceedings of the 59th American Helicopter Society Annual Forum*, American Helicopter Society, Alexandria, VA, June 2002.

[23]Xin, H., and He, C., "A Combined Technique for Inverse Simulation Applied to Rotorcraft Shipboard Operations," *Proceedings of the 58th American Helicopter Society Annual Forum*, American Helicopter Society, Alexandria, VA, June 2002.

[24]Kleinman, D. L., Baron, S., and Levison, W. H., "An Optimal Control Model of Human Response Part I: Theory and Validation," *Automatica*, Vol. 6, No. 3, 1970, pp. 357–369.

[25]Bradley, R., and Turner, G., "Simulation of the Human Pilot applied at the Helicopter/Ship Dynamic Interface," *Proceedings of the 55th American Helicopter Society Annual Forum*, American Helicopter Society, Alexandria, VA, May 1999, pp. 677–688.

[26]Hess, R. A., "Feedback Control Models—Manual Control and Tracking," *Handbook of Human Factors and Ergonomics*, 2nd ed., edited by G. Salevendy, Wiley, New York, 1997, Chap. 9.5.

[27]Lee, D., and Horn, J. F., "Simulation and Control of Helicopter Shipboard Launch and Recovery Operations," *Proceedings of the American Helicopter Society Flight Controls and Crew System Design Specialists' Meeting*, American Helicopter Society, Alexandria, VA, Oct. 2002.

[28]Labows, S. J., Tischler, M. B., and Blanken, C. L., "UH-60 Black Hawk Disturbance Rejection Study for Hover/Low Speed Handling Qualities Criteria and Turbulence Modeling," *Proceedings of the 56th American Helicopter Society Annual Forum*, American Helicopter Society, Alexandria, VA, May 2000.

[29]Howlett, J. J., "UH-60A BLACK HAWK Engineering Simulation Program: Volume I—Mathematical Model," NASA CR-177542, USAAVSCOM TR 89-A-001, Sept. 1989.

[30]He, C., "Development and Application of a Generalized Dynamic Wake Theory of Lifting Rotors," Ph.D. Dissertation, School of Aerospace Engineering, Georgia Inst. of Technology, Atlanta, July 1989.

[31]Xin, H., Prasad, J. V. R., and Peters, D., "Dynamic Inflow Modeling for Simulation of a Helicopter Operating in Ground Effect," AIAA Paper 99-4114, Aug. 1999.

[32]Dahl, H. J., and Faulkner, A. J., "Helicopter Simulation in Atmospheric Turbulence," *Proceedings of the 4th European Rotorcraft Forum*, Sept. 1978.

[33]Clement, W. F., Gorder, P. J., and Jewell, W. F., "Development of a Real-Time Simulation of a Ship-Correlated Airwake Model Interfaced with a Rotorcraft Dynamic Model," The Naval Air Systems Command, TR-91-C-0176, Patuxent River, MD, 1991.

[34]Modi, A., Sezer-Uzol, N., Long, L. N., and Plassmann, P. E., "Scalable Computational Steering System for Visualization of Large-Scale CFD Simulations," AIAA Paper 2002-2750, June 2002.

[35]Modi, A., Sezer-Uzol, N., Long, L. N., and Plassmann, P. E., "Scalable Computational Steering System for Visualization of Large-Scale Fluid Dynamics Simulations," Journal of Aircraft (to be published).

[36]Souliez, F. J., "Parallel Methods for the Computation of Unsteady Separated Flows Around Complex Geometries," Ph.D. Dissertation, Dept. of Aerospace Engineering, The Pennsylvania State Univ., University Park, PA, Aug. 2002.

[37]Jindal, S., Long, L. N., Plassmann, P. E., and Sezer-Uzol, N., "Large Eddy Simulations Around a Sphere Using Unstructured Grids," AIAA Paper 2004-2228, June 2004.